Pervasive beyond Room-Temperature Ferromagnetism in a Doped van der Waals Magnet

Xiang Chen,[1,2,*] Yu-Tsun Shao,[3] Rui Chen,[4,1] Sandhya Susarla,[4,1] Tom Hogan,[5] Yu He,[6,2,1] Hongrui Zhang,[4] Siqi Wang,[7] Jie Yao,[4,1] Peter Ercius,[8] David A. Muller,[3,9] Ramamoorthy Ramesh,[4,1,2] and Robert J. Birgeneau[2,1,4,†]

[1]*Materials Sciences Division, Lawrence Berkeley National Lab, Berkeley, California 94720, USA*
[2]*Physics Department, University of California, Berkeley, California 94720, USA*
[3]*School of Applied and Engineering Physics, Cornell University, Ithaca, New York 14853, USA*
[4]*Department of Materials Science and Engineering, University of California, Berkeley, California 94720, USA*
[5]*Quantum Design, Inc., San Diego, California 92121, USA*
[6]*Department of Applied Physics, Yale University, New Haven, Connecticut, 06511, USA*
[7]*NSF Nanoscale Science and Engineering Center (NSEC), 3112 Etcheverry Hall, University of California, Berkeley, California 94720, USA*
[8]*The Molecular Foundry, Lawrence Berkeley National Laboratory, Berkeley, California 94720, USA*
[9]*Kavli Institute at Cornell for Nanoscale Science, Cornell University, Ithaca, New York 14853, USA*

(Received 4 December 2021; accepted 28 April 2022; published 26 May 2022)

The existence of long-range magnetic order in low-dimensional magnetic systems, such as the quasi-two-dimensional van der Waals (vdW) magnets, has attracted intensive studies of new physical phenomena. The vdW Fe_NGeTe_2 ($N = 3$, 4, 5; FGT) family is exceptional, owing to its vast tunability of magnetic properties. In particular, a ferromagnetic ordering temperature (T_C) above room temperature at $N = 5$ (F5GT) is observed. Here, our study shows that, by nickel (Ni) substitution of iron in F5GT, a record high $T_C = 478(6)$ K is achieved. Importantly, pervasive, beyond room-temperature ferromagnetism exists in almost the entire doping range of the phase diagram of Ni-F5GT. We argue that this striking observation in Ni-F5GT can be possibly due to several contributing factors, including increased 3D magnetic couplings due to the structural alterations.

DOI: 10.1103/PhysRevLett.128.217203

Introduction.—Spontaneous symmetry breaking is forbidden at nonzero temperatures in isotropic spin systems with dimensions $d \leq 2$ [1,2]. Long-range magnetic order in materials with reduced dimensionality can still be stabilized via both magnetic anisotropy and weak three-dimensional (3D) magnetic couplings [3–5]. In quasi-two-dimensional (quasi-2D) Heisenberg magnets, such as the van der Waals (vdW) bonded materials, the ordering process typically occurs as follows [6–8]. At the highest temperature, the system is expected to exhibit 2D, classical isotropic magnetic correlations. As the temperature T is lowered, the correlation length grows exponentially with $1/T$, and at sufficiently large length scales, there is inevitably a crossover from 2D Heisenberg to 3D Ising or XY behavior followed by a phase transition to the 3D long-range magnetic order. The details of the crossover depend on the strength of the 3D magnetic interactions and the symmetry and strength of the magnetic anisotropy. van der Waals materials represent exciting realizations of these phenomena, plus they contain the broad prospect of important technological applications [9–15].

Among the prominent bulk vdW materials for studying quasi-2D magnetism, such as $Cr_2Ge_2Te_6$ [16,17], CrI_3 [18,19], Fe_3GeTe_2 (F3GT) [20–25], and $CrTe_2$ [26,27], the F3GT system is exceptional, owing to the coupling between the electronic and magnetic degrees of freedom and its remarkable tunability. The bulk form of F3GT has a ferromagnetic (FM) transition temperature $T_C \sim 230$ K, which can be readily enhanced up to room temperature (RT) by either patterning the microstructure or applying ionic gating [28,29]. By intercalating more iron (Fe) into F3GT, i.e., Fe_NGeTe_2 ($N = 4$ for F4GT or 5 for F5GT) [30–32], the marked effects are the elevated T_C up to RT and enhanced magnetization, while only moderately increasing the magnetic moment size [30,32,33]. The F5GT compound is particularly interesting because of its advantageous characteristics for potential RT spintronic applications, including a T_C above RT (~315 K), large magnetization (~700 kA/m), strong spin lattice coupling [32,33], and exotic magnetic textures [34,35].

To achieve practical applications of the quasi-2D magnetic materials, one common theme is to strengthen the FM and enhance the T_C of the vdW magnets. Some proven avenues to dramatically raise the T_C include gating [28,36], applying pressure or strain [37], ion intercalation, or carrier doping [38,39]. By cobalt (Co) substitution of F5GT, i.e., $(Fe_{1-x}Co_x)_{5+\delta}GeTe_2$ (Co-F5GT), the magnetic ordering temperature is further increased to ~360 K, along with the evolution of the magnetic ground state [40–43]. More strikingly, at $x = 0.5$ of Co-F5GT, a novel wurtzite-type

polar magnetic metal was discovered, along with the Néel-type skyrmion lattice at RT [42,43]. The aforementioned discoveries of the F5GT system highlight its immense tunability and capacity for applications in next-generation spintronics.

In this Letter, we report pervasive, well-beyond room-temperature FM in the F5GT vdW magnet with nickel (Ni) substitution, i.e., $(Fe_{1-x}Ni_x)_{5+\delta}GeTe_2$ (Ni-F5GT). Strikingly, a record high $T_C = 478(6)$ K is reached at a Ni doping level of $x = 0.36(2)$. In addition, the FM order persists robustly against Ni replacement until $x \sim 0.86(1)$, beyond which only weak paramagnetism exists. Several factors might be relevant for the dramatic enhancement of the FM in Ni-F5GT.

The Ni-F5GT single crystals were grown by the chemical vapor transfer method [32,33,44]. The exact Ni doping level x and total cation count per formula unit (f.u.) $5 + \delta$ were verified by energy-dispersive x-ray (EDX) spectroscopy (see Fig. S1 in the Supplemental Material [44]). The lattice and atomic structure of Ni-F5GT were investigated by a combination of techniques, including powder and/or single crystal x-ray diffraction (XRD) and high-angle annular dark-field scanning transmission electron microscopy (HAADF STEM). Magnetization measurements were performed via a commercial Quantum Design MPMS3.

The unit cell of F5GT is composed of three identical layers (stacks) with the rhombohedral layer stacking (space group $R\bar{3}m$) labeled as ABC stacking [32]. Upon introducing Ni into F5GT, such as at $x = 0.19(1)$, the crystal structure undergoes a transition from ABC stacking to AA stacking [space group $P\bar{3}m1$ illustrated in Fig. 1(a)], as confirmed by single crystal XRD (see Fig. S2 in the Supplemental Material [44]). The AA-stacking order is also verified by HAADF STEM images at other doping levels (Fig. 2 and Supplemental Material Fig. S5 [44]). When viewed along the $[1\ \ 1\ \ 0]$ direction, the identical layers stack exactly on top of each other along the c direction and are separated by a vdW spatial gap. Within each layer (stack), the center germanium (Ge, blue symbols) atom is surrounded by three different sites of iron (Fe1, Fe2, and Fe3, green) atoms which are further protected by the outer Te (purple) atoms, i.e., forming a Te-Fe1-Fe3-Fe2-Ge-Fe2-Fe3-Fe1-Te planelike (labeled as TGT plane) structure.

With increasing Ni doping in Ni-F5GT, the excess cation count δ gradually increases from $\delta \sim 0$ at $x = 0$ to $\delta \sim 0.5$ at $x \sim 0.3$ [labeled as region (I) with $0 \le x \le 0.3$] and saturates when $x > 0.3$ (see Fig. S1 in the Supplemental Material [44]). Interestingly, in the intermediate doping range $0.36(2) \le x \le 0.86(1)$ [region (II)], although the sample still maintains the AA stacking, two types of domains coexist, as evidenced from the splitting of the $(0\ \ 0\ \ L)$ peaks from the XRD measurements [Fig. 1(b)], the direct atomic visualization from the HAADF STEM images (Fig. 2 and Supplemental Material Fig. S5 [44]),

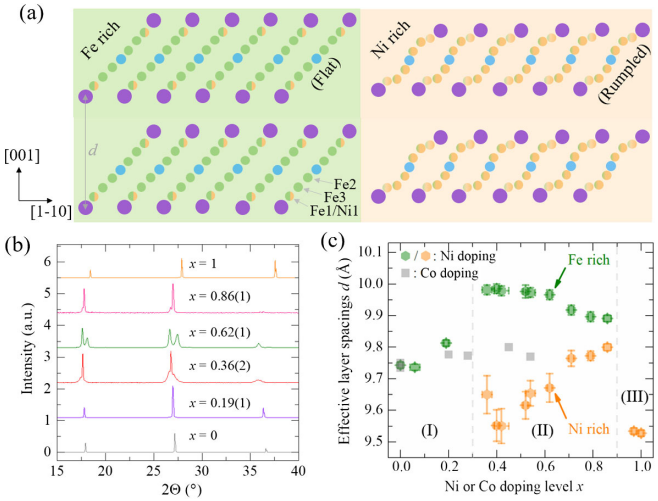

FIG. 1. (a) Illustration of the AA-stacking order of both the Fe-rich and Ni-rich domains in Ni doped Fe_5GeTe_2 (Ni-F5GT) (green symbols, Fe; orange, Ni; purple, Te; blue, Ge) [44]. (b) The $(0\ \ 0\ \ L)$-type of peaks of Ni-F5GT at select Ni doping levels x. (c) Effective layer spacing d as a function of Ni doping (colored symbols) or Co doping (gray symbols [42]) in $Fe_{5+\delta}GeTe_2$. Vertical dashed lines indicate different regions in Ni-F5GT.

and the STEM EDX maps (Fig. 2 and Supplemental Material Fig. S4 [44]). As an example, at $x = 0.36(2)$ [Fig. 2 and illustrated in Fig. 1(a)] the two types of domains correspond to the Fe-rich domains [Fig. 2(c)] and Ni-rich domains [Fig. 2(d)], respectively. In the Fe-rich domains, the TGT planes are almost flat and more extended in space, while the TGT planes are rumpled in the Ni-rich domains. Because of the contrasting local atomic arrangements of the Fe and Ni atoms within the TGT planes, the effective layer spacing d of either the Fe-rich or Ni-rich domain shows a strong deviation from the value at $x = 0$ [Fig. 1(c)]. This strong alteration may have a dramatic impact on the electronic and/or magnetic properties of Ni-F5GT.

While the Ni-F5GT samples are still metallic (see Fig. S6 in the Supplemental Material [44]), the magnetic properties are strongly influenced by Ni substitution (Fig. 3 and Supplemental Material Fig. S7 [44]). With moderate Ni replacement, the T_C of Ni-F5GT is already considerably enhanced [Figs. 3(a) and 3(b)]. For instance, at $x = 0.19(1)$, the experimentally determined $T_C = 395(6)$ K already approaches 400 K [Fig. 3(a)]. Meanwhile, the Ising spin moment switches to the in-plane direction and seems to remain so until $x \sim 0.86(1)$ [Fig. 3(e) and Supplemental Material Fig. S7 [44]]. Upon further increasing the Ni content, a record high $T_C = 478(6)$ K is achieved at $x = 0.36(2)$, together with the maximum in-plane ($H_C^{ab} \approx 500$ Oe) and out-of-plane ($H_C^{c} \approx 1600$ Oe) coercive fields [Figs. 3(c) and 3(f) and Supplemental Material Fig. S7 [44]]. After reaching the maximum T_C in Ni-F5GT, the FM order is only gradually weakened by further Ni doping. Strikingly, even at $x = 0.86(1)$, the

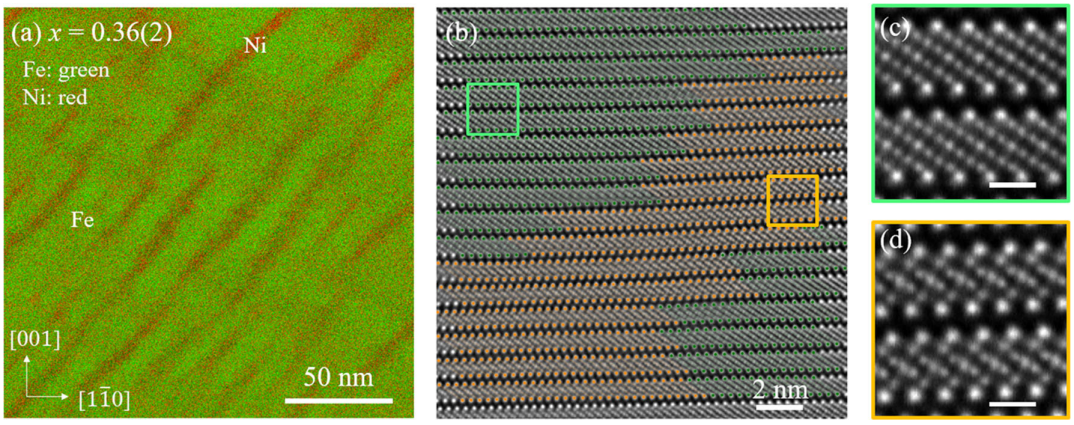

FIG. 2. Nanoscale phase separation of Ni-F5GT at $x = 0.36(2)$. (a) Energy-dispersive x-ray spectroscopy map showing both the Fe-rich (green) and Ni-rich (red) regions. (b)–(d) Atomic resolution HAADF STEM image demonstrating the two types of domains. The enlarged (c) Fe-rich and (d) Ni-rich domains show flat and rumpled atomic planes, respectively. The Te-Te planes in (b) are color coded based on the number and the rumpling of the atomic layers. Scale bars in (c),(d), 5 Å.

as-grown sample of Ni-F5GT maintains an above room-temperature $T_C \approx 380$ K, which is only lowered and stabilized at 220 or 150 K, depending on how the sample is thermally cycled above its original T_C (see Supplemental Material Fig. S8 [44]). Only beyond this point of further Ni replacement [$0.86(1) < x \leq 1$, region (III)], the FM order of Ni-F5GT is completely suppressed, rendering the weak paramagnetism accompanied by the adoption of a different, layered tetragonal structure (space group $I4/mmm$) as $Ni_{5.5}GeTe_2$ [45].

The saturation magnetic moment per f.u. of Ni-F5GT at 2 K decreases approximately linearly with increasing Ni content [Figs. 3(c) and 3(e) and Supplemental Material Fig. S7 [44]] from $\sim 10\ \mu_B$/f.u. at $x = 0$ to nearly zero

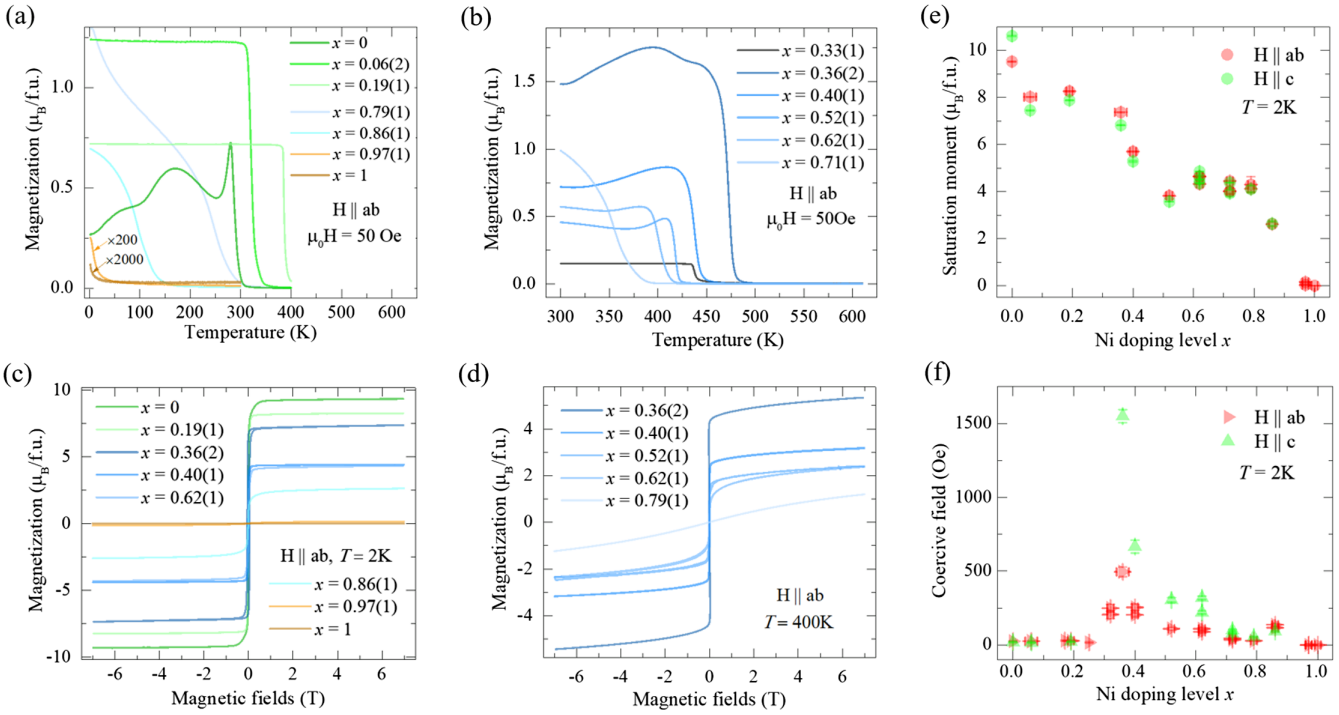

FIG. 3. Magnetization data of Ni-F5GT at select Ni doping level x. (a),(b) Temperature-dependent magnetization of Ni-F5GT (external in-plane magnetic field is 50 Oe). For clarity, the magnetization data at $x = 0.97(1)$ and $x = 1$ are multiplied by 200 and 2000, respectively. (c),(d) In-plane isothermal magnetization at $T = 2$ K (c) and $T = 400$ K (d), respectively. (e) Saturation moment per formula unit at 2 K under the magnetic field of 7 T. (f) Coercive fields extracted from the isothermal magnetization at $T = 2$ K. In (e) and (f), the magnetic field is applied along the ab-plane (red symbols) or c direction (green symbols).

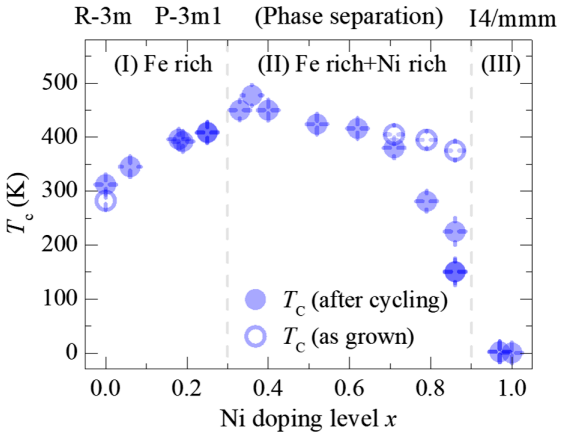

FIG. 4. Ni doping level x-dependent T_C in Ni-F5GT. Empty symbols, T_C for as-grown samples; solid symbols, T_C after thermal cycling. Vertical dashed lines indicate different regions in Ni-F5GT.

(weakly paramagnetic) at $x = 1$. This implies that the Ni dopants are not magnetic and only dilute the FM in Ni-F5GT. Surprisingly, the magnetic ordering temperature T_C does not follow this expected trend (Fig. 4). Instead, pervasive, above room-temperature FM exists almost over the entire range of the phase diagram [$0 \leq x \leq 0.79(1)$]. Particularly, in region (I) of the phase diagram of Ni-F5GT, the T_C shows a strong, positive deviation from the Vegard's law behavior (i.e., a dilution of the magnetic component), thus suggesting additional factors might be present for the unusual evolution of T_C. Our study demonstrates the remarkable Ni enhanced FM in Ni-F5GT, as summarized in Fig. 4, where three different regions are categorized based on the structural and magnetic characterization.

The unique feature of Ni-F5GT is the immense impact on the lattice and magnetism by Ni substitution, including the radical change of the layer spacing d [Fig. 1(c)] and the local atomic arrangements [Figs. 1(a) and 2, and Supplemental Material Figs. S2–S5 [44]], as compared to F5GT or Co-F5GT [32,42]. It is evident that the change of the layer spacing d in Ni-F5GT is significantly more pronounced than its evolution in Co-F5GT. Importantly, the layer spacing d of the Fe-rich domains [green symbols in Fig. 1(c)] closely tracks the evolution of T_C in Ni-F5GT at $0 \leq x \leq 0.86(1)$ (Fig. 4). This is supported by the experimental observation that the Fe-rich domains maintain the AA-stacking order with the straight-and-flat TGT planes over a broad Ni doping range $0 < x \leq 0.86(1)$ and thus may be mainly responsible for the robust FM in Ni-F5GT. The Ni dopants are also indispensable for donating electrons to the system and forming the Ni-rich domains in region (II), which help preserve the Fe-rich domains. This phase separation in region (II) naturally explains the domain pinning enhanced coercive fields [Fig. 3(f)]. Meanwhile, the preserved Fe-rich domains maintain the robust T_C of Ni-F5GT in this region.

Our work on Ni-F5GT reveals a complicated yet intriguing system in which the lattice, electronic, and magnetic degrees of freedom are closely intertwined. To understand the enhancement of FM in Ni-F5GT, especially the region (I) (Fig. 4), it is necessary to consider the possible effects of both electron doping and structural alteration by Ni replacement. Carrier doping is often seen to be detrimental to the correlation-induced long-range magnetic order, as recognized in the unconventional superconductors, such as the cuprates and iron pnictides [46,47]. For the itinerant FM, charge doping can, in some cases, help meet the Stoner criterion and actually promote magnetic order [48]. The related F3GT system, which may also apply to F5GT, has both itinerant and localized spin moment contributions to the magnetism [21,23–25,28,49,50]. Hence, the ordering temperature of F3GT can be elevated by electrostatic gating of its thin layer form [28,36]. In Ni-F5GT, the electrons provided by the Ni dopants may greatly influence the electronic band structure and the density of states near the Fermi level (E_F). Alternatively, the magnetic exchange coupling $J_{i,j}$ between spins $\boldsymbol{S}_i$ and $\boldsymbol{S}_j$ on sites i and j might also be altered via the Ruderman-Kittel-Kasuya-Yosida exchange since the electronic structure is likely altered substantially by Ni doping [25,28,51,52]. Altogether, the itinerant FM might also be enhanced by electron doping in Ni-F5GT.

Now focusing on the localized spin moments and considering a simple Heisenberg model with a weak magnetic anisotropy in which the magnetic contributions from the itinerant FM can also be effectively mapped into the Hamiltonian [28,53]:

$$H = \sum_{i<j} J_{i,j} \boldsymbol{S}_i \cdot \boldsymbol{S}_j - \sum_i A(S_i^z)^2. \tag{1}$$

Here, A is the single-ion anisotropy ($A > 0$ for Ising spin moment). Since A is small and close to zero in Ni-F5GT [33], a mean-field treatment results in the magnetic transition temperature [12,28]:

$$T_C = \frac{S(S+1)}{3k_B}(z_{\mathrm{NN}} J_{\mathrm{NN}} + \cdots), \tag{2}$$

where z_{NN} is the coordination number of the nearest-neighboring sites, S is the magnetic spin quantum number, and J_{NN} the nearest-neighbor exchange coupling. On the mean-field level, a larger z_{NN} or J_{NN} promises a larger T_C. Perhaps this is why the ordering temperature in Fe_NGeTe_2 is quickly increased from $T_C \sim 230$ K at $N = 3$ to $T_C \sim 317$ K at $N = 5$ [20,21,30,32,33]. In Ni-F5GT, since the average magnetic moment per Fe is almost unchanged and the in-plane FM indicates a small yet negative A [Fig. 3(e) and Supplemental Material Fig. S7 [44]], neither S nor A is responsible for the enhancement of the FM. However, the structural alterations may affect both z_{NN} and $J_{i,j}$, and

therefore are strong candidates for explaining the further enhanced T_C.

First, a small increment of δ is observed for lightly Ni doped F5GT [region (I) in Fig. 4 and Supplemental Material Fig. S1 [44]]. One direct consequence is the larger site occupancy of the Fe1 site, which is up to ~75% at $x \sim 0.3$ as compared to a maximum of ~50% at $x = 0$. Considering that the Fe1—Fe3 bond length is the shortest among all of the direct Fe—Fe bonds (see Fig. S3 in the Supplemental Material [44]), the Fe1 site might be critical for determining the T_C in Ni-F5GT. Therefore, a larger δ, which implies a greater z_{NN} of the Fe1 site, might promote a higher T_C [Eq. (2)]. Second, with more Ni substitution in region (I), the explicit effect is that the TGT planes of the Fe-rich domains are becoming more flat and extended in space [Fig. 2(c), and Supplemental Material Figs. S3, S5 (c), and S5(e) [44]]. Microscopically, other than the small spatial rearrangements of the Fe2 and Fe3 sites, it is the Fe1 site that is becoming increasingly distant from the Fe3 site along the c direction while keeping the Fe—Fe bond lengths nearly unchanged (see Supplemental Material Fig. S3 [44]). This explains the enlargement of the layer spacing d [Fig. 1(c)], which positively correlates with the T_C in Ni-F5GT. Understandably, the intralayer and interlayer exchange coupling, especially these related to the Fe1 site, might be effectively strengthened, which render the 3D magnetic interactions stronger and eventually lead to the enhancement of T_C in Ni-F5GT.

In summary, our work reveals a new arena for studying the vdW magnetic metals with strong room-temperature ferromagnetism. A record high ferromagnetic order with a $T_C = 478(6)$ K is realized in Ni-F5GT at $x = 0.36(2)$. Albeit with the nonmagnetic dilution, several factors are speculated to assist the pervasive, well-above room-temperature FM in Ni-F5GT. Candidate contributors include the increased site occupancy, structural modifications altered magnetic exchange couplings, and the electron doping effect. Clearly, as stated, these ideas are purely speculative and require much more thorough investigation. Although further research is needed to understand fully the mechanism of the enhanced magnetism, our study highlights that the Ni-F5GT system is an extremely rare example of strongly enhanced ferromagnetism, despite the detrimental factors such as the nonmagnetic dilution and electron doping effects introduced by Ni dopants. In addition, Ni-F5GT offers unique or alternative avenues toward enhanced coercivity, varying length scale of phase separation, thermal cycling influenced T_C, and potential relevance to skyrmionics in F5GT and other related vdW magnets [40–43].

X. C. wishes to thank Nicholas S. Settineri and Weiwei Xie for some single crystal XRD measurement and acknowledge the Applications Group at Quantum Design for their contribution of high-temperature (300–600 K) magnetization measurements to this work. Work at Lawrence Berkeley National Laboratory was funded by the U.S. Department of Energy, Office of Science, Office of Basic Energy Sciences, Materials Sciences and Engineering Division under Contract No. DE-AC02-05-CH11231 within the Quantum Materials Program (No. KC2202). Y. T. S., H. Z., and D. A. M. acknowledge financial support from the Department of Defense, Air Force Office of Scientific Research under Grant No. FA9550-18-1-0480. R. C. and J. Y. acknowledge the support by Intel Corporation under a grant titled Valleytronics Center. The electron microscopy studies were performed at the Cornell Center for Materials Research, a National Science Foundation (NSF) Materials Research Science and Engineering Centers program (No. DMR 1719875). The microscopy work at Cornell was supported by the NSF PARADIM Grant No. DMR-2039380, with additional support from Cornell University, the Weill Institute, and the Kavli Institute at Cornell. S. S. acknowledges the help from Dr. Rohan Dhall and is supported by the Quantum Materials Program under the Basic Energy Sciences, Department of Energy. The microscopy work was performed at Molecular Foundry that is supported by the Office of Science, Office of Basic Energy Sciences, of the U.S. Department of Energy under Contract No. DE-AC02-05CH11231. The devices for transport measurements were fabricated in the UC Berkeley Marvell Nanofabrication Laboratory.

*xiangchen@berbeley.edu
†robertjb@berkeley.edu

[1] N. D. Mermin and H. Wagner, Absence of Ferromagnetism or Antiferromagnetism in One- or Two-Dimensional Isotropic Heisenberg Models, Phys. Rev. Lett. **17**, 1133 (1966).
[2] P. C. Hohenberg, Existence of long-range order in one and two dimensions, Phys. Rev. **158**, 383 (1967).
[3] L. Onsager, Crystal statistics. I. A two-dimensional model with an order-disorder transition, Phys. Rev. **65**, 117 (1944).
[4] J. L. Lado and J. Fernández-Rossier, On the origin of magnetic anisotropy in two dimensional CrI_3, 2D Mater. **4**, 035002 (2017).
[5] D.-H. Kim, K. Kim, K.-T. Ko, J. H. Seo, J. S. Kim, T.-H. Jang, Y. Kim, J.-Y. Kim, S.-W. Cheong, and J.-H. Park, Giant Magnetic Anisotropy Induced by Ligand *LS* Coupling in Layered Cr Compounds, Phys. Rev. Lett. **122**, 207201 (2019).
[6] J. Als-Nielsen, R. J. Birgeneau, H. J. Guggenheim, and G. Shirane, Critical behaviour of a two-dimensional random antiferromagnet: $Rb_2Mn_{0.5}Ni_{0.5}F_4$, J. Phys. C **9**, L121 (1976).
[7] S. Chakravarty, B. I. Halperin, and D. R. Nelson, Two-dimensional quantum Heisenberg antiferromagnet at low temperatures, Phys. Rev. B **39**, 2344 (1989).
[8] R. J. Birgeneau, M. Greven, M. A. Kastner, Y. S. Lee, B. O. Wells, Y. Endoh, K. Yamada, and G. Shirane, Instantaneous spin correlations in La_2CuO_4, Phys. Rev. B **59**, 13788 (1999).

[9] J. M. Kosterlitz and D. J. Thouless, Ordering, metastability and phase transitions in two-dimensional systems, J. Phys. C **6**, 1181 (1973).

[10] J.-G. Park, Opportunities and challenges of 2D magnetic van der Waals materials: Magnetic graphene?, J. Phys. Condens. Matter **28**, 301001 (2016).

[11] K. S. Burch, D. Mandrus, and J.-G. Park, Magnetism in two-dimensional van der Waals materials, Nature (London) **563**, 47 (2018).

[12] M. Gibertini, M. Koperski, A. F. Morpurgo, and K. S. Novoselov, Magnetic 2D materials and heterostructures, Nat. Nanotechnol. **14**, 408 (2019).

[13] C. Gong and X. Zhang, Two-dimensional magnetic crystals and emergent heterostructure devices, Science **363**, eaav4450 (2019).

[14] M.-C. Wang, C.-C. Huang, C.-H. Cheung, C.-Y. Chen, S. G. Tan, T.-W. Huang, Y. Zhao, Y. Zhao, G. Wu, Y.-P. Feng, H.-C. Wu, and C.-R. Chang, Prospects and opportunities of 2D van der Waals magnetic systems, Ann. Phys. (Berlin) **532**, 1900452 (2020).

[15] L. Du, T. Hasan, A. Castellanos-Gomez, G.-B. Liu, Y. Yao, C. N. Lau, and Z. Sun, Engineering symmetry breaking in 2D layered materials, Nat. Rev. Phys. **3**, 193 (2021).

[16] V. Carteaux, D. Brunet, G. Ouvrard, and G. Andre, Crystallographic, magnetic and electronic structures of a new layered ferromagnetic compound $Cr_2Ge_2Te_6$, J. Phys. Condens. Matter **7**, 69 (1995).

[17] C. Gong, L. Li, Z. Li, H. Ji, A. Stern, Y. Xia, T. Cao, W. Bao, C. Wang, Y. Wang, Z. Q. Qiu, R. J. Cava, S. G. Louie, J. Xia, and X. Zhang, Discovery of intrinsic ferromagnetism in two-dimensional van der Waals crystals, Nature (London) **546**, 265 (2017).

[18] M. A. McGuire, H. Dixit, V. R. Cooper, and B. C. Sales, Coupling of crystal structure and magnetism in the layered, ferromagnetic insulator CrI_3, Chem. Mater. **27**, 612 (2015).

[19] B. Huang, G. Clark, E. Navarro-Moratalla, D. R. Klein, R. Cheng, K. L. Seyler, D. Zhong, E. Schmidgall, M. A. McGuire, D. H. Cobden, W. Yao, D. Xiao, P. Jarillo-Herrero, and X. Xu, Layer-dependent ferromagnetism in a van der Waals crystal down to the monolayer limit, Nature (London) **546**, 270 (2017).

[20] H.-J. Deiseroth, K. Aleksandrov, C. Reiner, L. Kienle, and R. K. Kremer, Fe_3GeTe_2 and Ni_3GeTe_2—Two new layered transition-metal compounds: Crystal structures, HRTEM investigations, and magnetic and electrical properties, Eur. J. Inorg. Chem. **2006**, 1561 (2006).

[21] B. Chen, J. Yang, H. Wang, M. Imai, H. Ohta, C. Michioka, K. Yoshimura, and M. Fang, Magnetic properties of layered itinerant electron ferromagnet Fe_3GeTe_2, J. Phys. Soc. Jpn. **82**, 124711 (2013).

[22] Z. Fei, B. Huang, P. Malinowski, W. Wang, T. Song, J. Sanchez, W. Yao, D. Xiao, X. Zhu, A. F. May, W. Wu, D. H. Cobden, J.-H. Chu, and X. Xu, Two-dimensional itinerant ferromagnetism in atomically thin Fe_3GeTe_2, Nat. Mater. **17**, 778 (2018).

[23] A. F. May, S. Calder, C. Cantoni, H. Cao, and M. A. McGuire, Magnetic structure and phase stability of the van der Waals bonded ferromagnet $Fe_{3-x}GeTe_2$, Phys. Rev. B **93**, 014411 (2016).

[24] K. Kim, J. Seo, E. Lee, K.-T. Ko, B. S. Kim, B. G. Jang, J. M. Ok, J. Lee, Y. J. Jo, W. Kang, J. H. Shim, C. Kim, H. W. Yeom, B. Il Min, B.-J. Yang, and J. S. Kim, Large anomalous Hall current induced by topological nodal lines in a ferromagnetic van der Waals semimetal, Nat. Mater. **17**, 794 (2018).

[25] Y. Zhang, H. Lu, X. Zhu, S. Tan, W. Feng, Q. Liu, W. Zhang, Q. Chen, Y. Liu, X. Luo, D. Xie, L. Luo, Z. Zhang, and X. Lai, Emergence of Kondo lattice behavior in a van der Waals itinerant ferromagnet, Fe_3GeTe_2, Sci. Adv. **4**, eaao6791 (2018).

[26] D. C. Freitas, R. Weht, A. Sulpice, G. Remenyi, P. Strobel, F. Gay, J. Marcus, and M. Núñez-Regueiro, Ferromagnetism in layered metastable 1*T*-$CrTe_2$, J. Phys. Condens. Matter **27**, 176002 (2015).

[27] X. Sun *et al.*, Room temperature ferromagnetism in ultra-thin van der Waals crystals of 1*T*-$CrTe_2$, Nano Res. **13**, 3358 (2020).

[28] Y. Deng, Y. Yu, Y. Song, J. Zhang, N. Z. Wang, Z. Sun, Y. Yi, Y. Z. Wu, S. Wu, J. Zhu, J. Wang, X. H. Chen, and Y. Zhang, Gate-tunable room-temperature ferromagnetism in two-dimensional Fe_3GeTe_2, Nature (London) **563**, 94 (2018).

[29] Q. Li *et al.*, Patterning-induced ferromagnetism of Fe_3GeTe_2 van der Waals materials beyond room temperature, Nano Lett. **18**, 5974 (2018).

[30] J. Seo *et al.*, Nearly room temperature ferromagnetism in a magnetic metal-rich van der Waals metal, Sci. Adv. **6**, eaay8912 (2020).

[31] J. Stahl, E. Shlaen, and D. Johrendt, The van der Waals ferromagnets $Fe_{5-\delta}GeTe_2$ and $Fe_{5-\delta-x}Ni_xGeTe_2$—crystal structure, stacking faults, and magnetic properties, Z. Anorg. Allg. Chem. **644**, 1923 (2018).

[32] A. F. May, D. Ovchinnikov, Q. Zheng, R. Hermann, S. Calder, B. Huang, Z. Fei, Y. Liu, X. Xu, and M. A. McGuire, Ferromagnetism near room temperature in the cleavable van der Waals crystal Fe_5GeTe_2, ACS Nano **13**, 4436 (2019).

[33] H. Zhang, R. Chen, K. Zhai, X. Chen, L. Caretta, X. Huang, R. V. Chopdekar, J. Cao, J. Sun, J. Yao, R. Birgeneau, and R. Ramesh, Itinerant ferromagnetism in van der Waals $Fe_{5-x}GeTe_2$ crystals above room temperature, Phys. Rev. B **102**, 064417 (2020).

[34] T. T. Ly, J. Park, K. Kim, H.-B. Ahn, N. J. Lee, K. Kim, T.-E. Park, G. Duvjir, N. H. Lam, K. Jang, C.-Y. You, Y. Jo, S. K. Kim, C. Lee, S. Kim, and J. Kim, Direct observation of Fe-Ge ordering in $Fe_{5-x}GeTe_2$ crystals and resultant helimagnetism, Adv. Funct. Mater. **31**, 2009758 (2021).

[35] Y. Gao, Q. Yin, Q. Wang, Z. Li, J. Cai, T. Zhao, H. Lei, S. Wang, Y. Zhang, and B. Shen, Spontaneous (anti)meron chains in the domain walls of van der Waals ferromagnetic $Fe_{5-x}GeTe_2$, Adv. Mater. **32**, 2005228 (2020).

[36] I. A. Verzhbitskiy, H. Kurebayashi, H. Cheng, J. Zhou, S. Khan, Y. P. Feng, and G. Eda, Controlling the magnetic anisotropy in $Cr_2Ge_2Te_6$ by electrostatic gating, National electronics review **3**, 460 (2020).

[37] D. Bhoi, J. Gouchi, N. Hiraoka, Y. Zhang, N. Ogita, T. Hasegawa, K. Kitagawa, H. Takagi, K. H. Kim, and Y. Uwatoko, Nearly Room-Temperature Ferromagnetism in a Pressure-Induced Correlated Metallic State of the van der

Waals Insulator $CrGeTe_3$, Phys. Rev. Lett. **127**, 217203 (2021).

[38] D. Weber, A. H. Trout, D. W. McComb, and J. E. Goldberger, Decomposition-induced room-temperature magnetism of the Na-intercalated layered ferromagnet $Fe_{3-x}GeTe_2$, Nano Lett. **19**, 5031 (2019).

[39] N. Wang, H. Tang, M. Shi, H. Zhang, W. Zhuo, D. Liu, F. Meng, L. Ma, J. Ying, L. Zou, Z. Sun, and X. Chen, Transition from ferromagnetic semiconductor to ferromagnetic metal with enhanced curie temperature in $Cr_2Ge_2Te_6$ via organic ion intercalation, J. Am. Chem. Soc. **141**, 17166 (2019).

[40] A. F. May, M.-H. Du, V. R. Cooper, and M. A. McGuire, Tuning magnetic order in the van der Waals metal Fe_5GeTe_2 by cobalt substitution, Phys. Rev. Mater. **4**, 074008 (2020).

[41] C. Tian, F. Pan, S. Xu, K. Ai, T. Xia, and P. Cheng, Tunable magnetic properties in van der Waals crystals $(Fe_{1-x}Co_x)_5GeTe_2$, Appl. Phys. Lett. **116**, 202402 (2020).

[42] H. Zhang, Y.-T. Shao, R. Chen, X. Chen, S. Susarla, D. Raftrey, J. T. Reichanadter, L. Caretta, X. Huang, N. S. Settineri, Z. Chen, J. Zhou, E. Bourret-Courchesne, P. Ercius, J. Yao, P. Fischer, J. B. Neaton, D. A. Muller, R. J. Birgeneau, and R. Ramesh, A room temperature polar magnetic metal, Phys. Rev. Mater. **6**, 044403 (2022).

[43] H. Zhang, D. Raftrey, Y.-T. Chan, Y.-T. Shao, R. Chen, X. Chen, X. Huang, J. T. Reichanadter, K. Dong, S. Susarla, L. Caretta, Z. Chen, J. Yao, P. Fischer, J. B. Neaton, W. Wu, D. A. Muller, R. J. Birgeneau, and R. Ramesh, Room-temperature skyrmion lattice in a layered magnet $(Fe_{0.5}Co_{0.5})_5GeTe_2$, Sci. Adv. **8**, eabm7103 (2022).

[44] See Supplemental Material at http://link.aps.org/supplemental/10.1103/PhysRevLett.128.217203 for additional data of sample synthesis, characterizations, transport measurements, magnetization, etc.

[45] H.-J. Deiseroth, F. Spirovski, C. Reiner, and M. Schlosser, Crystal structures of nickel germanium selenide, $Ni_{5.45}GeSe_2$, and nickel germanium telluride, $Ni_{5.45}GeTe_2$, Z. Kristallogr. **222**, 171 (2007).

[46] P. A. Lee, N. Nagaosa, and X.-G. Wen, Doping a Mott insulator: Physics of high-temperature superconductivity, Rev. Mod. Phys. **78**, 17 (2006).

[47] P. Dai, Antiferromagnetic order and spin dynamics in iron-based superconductors, Rev. Mod. Phys. **87**, 855 (2015).

[48] J. Huang, Z. Wang, H. Pang, H. Wu, H. Cao, S.-K. Mo, A. Rustagi, A. F. Kemper, M. Wang, M. Yi, and R. J. Birgeneau, Flat-band-induced itinerant ferromagnetism in $RbCo_2Se_2$, Phys. Rev. B **103**, 165105 (2021).

[49] S. Calder, A. I. Kolesnikov, and A. F. May, Magnetic excitations in the quasi-two-dimensional ferromagnet $Fe_{3-x}GeTe_2$ measured with inelastic neutron scattering, Phys. Rev. B **99**, 094423 (2019).

[50] X. Xu, Y. W. Li, S. R. Duan, S. L. Zhang, Y. J. Chen, L. Kang, A. J. Liang, C. Chen, W. Xia, Y. Xu, P. Malinowski, X. D. Xu, J.-H. Chu, G. Li, Y. F. Guo, Z. K. Liu, L. X. Yang, and Y. L. Chen, Signature for non-Stoner ferromagnetism in the van der Waals ferromagnet Fe_3GeTe_2, Phys. Rev. B **101**, 201104(R) (2020).

[51] J. Seo, E. S. An, T. Park, S.-Y. Hwang, G.-Y. Kim, K. Song, W.-s. Noh, J. Y. Kim, G. S. Choi, M. Choi, E. Oh, K. Watanabe, T. Taniguchi, J. H. Park, Y. J. Jo, H. W. Yeom, S.-Y. Choi, J. H. Shim, and J. S. Kim, Tunable high-temperature itinerant antiferromagnetism in a van der Waals magnet, Nat. Commun. **12**, 2844 (2021).

[52] M. Zhao, B.-B. Chen, Y. Xi, Y. Zhao, H. Xu, H. Zhang, N. Cheng, H. Feng, J. Zhuang, F. Pan, X. Xu, W. Hao, W. Li, S. Zhou, S. X. Dou, and Y. Du, Kondo holes in the two-dimensional itinerant Ising ferromagnet Fe_3GeTe_2, Nano Lett. **21**, 6117 (2021).

[53] R. E. Prange and V. Korenman, Local-band theory of itinerant ferromagnetism. IV. Equivalent Heisenberg model, Phys. Rev. B **19**, 4691 (1979).